



# Influence of coupling mechanism of loose layer and fault on multi-physical fields in mining areas

Jin Luo<sup>1,2</sup> · Yingming Li<sup>1,2</sup> · Xiangrui Meng<sup>1,2</sup> · Qingbiao Guo<sup>1,3</sup> · Guangming Zhao<sup>1,2</sup>

Received: 24 November 2022 / Revised: 26 March 2023 / Accepted: 10 August 2023  
© The Author(s) 2023

## Abstract

Coal mining under the geological conditions of a loose layer will lead to the intensification of surface movement and deformation, and mining under the geological conditions of a fault will lead to the living slip of a fault. Mining under both conditions will have a great impact on the safety of coal production. To reveal the evolution law of the coupling mechanism of loose layer and fault on the multi-physical fields of overburden, the numerical simulation method is used to simulate the coupling of loose layer and fault with different thicknesses, analyze the changes of vertical stress on the key strata, the changes of surface subsidence, the evolution of elastic energy on the fault zone and the changes of activated slip area of the fault zone. The simulation analysis shows that the vertical stress change trend of the key strata gradually changes from the "V" shape to the "W" shape at the beginning of mining, and the vertical stress concentration will occur at the fault. The loose layer will promote surface subsidence, and the fault will hinder the surface subsidence to a certain extent. The loose layer and the fault alternately affect the surface subsidence. The elastic energy accumulation on the key strata is mainly concentrated on both sides of the goaf. The elastic energy in the center of the goaf is dissipated. The elastic energy accumulation in the fault zone starts from the shallowly buried fault and gradually develops to the deeply buried fault. The instability of fault activation has gone through the initial stage of activation—the intensification stage of activation—the stable stage of activation. Under the working conditions of no loose layer, thin loose layer, and thick loose layer, the fault zone is the first to undergo living slip, and under the action of an extra-thick loose layer, there is a certain lag in the activation slip of the fault zone.

**Keywords** Loose layer · Fault · Vertical stress · Surface subsidence · Elastic energy · Activated slip

## 1 Introduction

Coal is the main energy in the world and plays an irreplaceable role in world economic development (Jiang et al. 2019a, b, c; Rahmatmand al. 2023). Against the background of increasing coal demand, the geological conditions of coal mining are becoming more and more complex (Wu et al.

2018; Lu et al. 2016; Jiang et al. 2019a, b, c). Faults and joints widely exist in the underground rock mass and directly affect the macro mechanical properties of rock mass, such as load resistance, deformation capacity, shear strength, etc. (Jiang et al. 2019a, b, c). The occurrence environment of complex geological structures such as faults is an important inducement for dynamic disasters such as rockburst (Rehcock Sander et al. 2018). Generally, when the coal mining working face is close to a fault, the fault that is initially in equilibrium will produce a series of chain effects under the influence of mining, such as fault stress concentration (Souque et al. 2019), and cracks and sinking steps will appear on the surface (Ścigała and Szafuła 2020). When there is a loose layer in the stratum with fault, the mining of coal resources will be more difficult. The loose and unstable structural characteristics of a loose layer will make the formation damage process more complex.

Wang et al. (2020) established the FLAC<sup>3D</sup> numerical model based on the geological conditions of the No. 6303

✉ Qingbiao Guo  
qbguoast@163.com

<sup>1</sup> State Key Laboratory of Mining Response and Disaster Prevention and Control in Deep Coal Mines, Anhui University of Science and Technology, Huainan 232001, Anhui, China

<sup>2</sup> School of Mining Engineering, Anhui University of Sciences and Technology, Huainan 232001, Anhui, China

<sup>3</sup> School of Spatial Informatics and Geomatics Engineering, Anhui University of Sciences and Technology, Huainan 232001, Anhui, China

working face of the Jisan Coal Mine of Yanzhou Mining Group and calculated it. They studied the blocking effect of fault on vertical stress, horizontal stress, and shear stress. The research shows that the stress concentration area on the fault zone will gradually expand to the hanging wall as the working face advances. Through experimental research, numerical simulation, and on-site microseismic monitoring Cai et al. (2021), verified the mechanism that the superposition of static stress and dynamic stress in the process of mining leads to fault activation and induced shock. Shen et al. (2021) found that the stress around the dam was abnormal due to the influence of the fault during the monitoring of the dam near a coal mine in Australia. The stress around the dam was redistributed, resulting in stress concentration in the hanging wall and stress release in the footwall. Fernández-Torres et al. (2022) found that fault activity has affected the ground subsidence of Mexico City for more than 100 years. The research results show that the ground bench subsidence caused by faults has occurred in the northeast part of Mexico City and the suburbs, and the maximum local subsidence has reached 423 mm/a. Brunori et al. (2015) studied the influence of thick loose layer sedimentation and fault existence through InSAR technology and field monitoring. The research results show that a 1.5 km long ground crack occurred in Halysco, Mexico, which led to the deformation of roads and the expansion of cracks in adjacent buildings. They believe that surface deformation and cracks are affected by both loose layers and faults. Cao et al. (2022) studied the working conditions of water inrush from coal seams when mining deep-buried coal seams under fault geological conditions and established a corresponding evaluation model for fault seepage barrier capacity. The results show that aquifers can threaten the stability of fault zones and have a certain impact on coal mining. Sainoki et al. (2014) took full account of various factors that may cause fault slip, established a fault model of the mineral deposit, and carried out dynamic numerical simulation analysis. The research results show that the fault will lead to slipping in the process of mining, which is easy to cause safety accidents in coal mining. When there is a loose layer on the surface, the surface subsidence has special characteristics compared with that when there is no loose layer. When there is a thick loose layer, the maximum surface subsidence value may be greater than the mining height of the coal seam (Garcia et al. 2022). During the coal seam mining process, the rock stratum will form a collapse zone, fracture zone, and bending zone (Shoab et al. 2022). Lai et al. (2021) used similar simulation experiments and numerical simulation experiments to analyze the overburden migration and the development of water-flowing fracture zone in the mining of three soft coal seams under thick loose beds. The research shows that the movement

of the loose layer presents a "Hyperbolic" shape, and the development of the water-conducting fracture zone has gone through five stages.

Based on the research of many scholars, it has been found that the existence of loose layer and faults will cause considerable security risks to coal mining, but how the overburdened multi-physical fields change when they are coupled will be the focus of this paper. In this paper, from the point of view of the coupling between loose layer and fault, a numerical simulation model is established to study the vertical stress variation law of key strata, surface subsidence characteristics, energy evolution of fault zone, and active slip surface product of fault zone when different loose layer thickness and fault coupling are in the process of mining. The purpose of this paper is to reveal the characteristics of the multi-physical field evolution of rock strata under special geological coupling, to provide theoretical guidance for safe and efficient mining of coal mines.

## 2 Numerical simulation

### 2.1 Numerical simulation model

This paper researches the evolution of the overburdened multi-physical fields caused by coal mining when only loose layers exist and when loose layers are coupled with faults. A numerical model is established with a length of 1200 m, a width of 1200 m, and a height of 300 m. The thickness of the coal is 5 m, the coal is horizontal, the thickness of the fault is 5 m and the dip angle of the fault is  $55^\circ$ . The grid size is  $30\text{ m} \times 30\text{ m}$ , with a total of 44,800 cells and 48,790 nodes. The excavation size of the model is  $400\text{ m} \times 360\text{ m}$ , the working face is 400 m long in direction and 360 m long in tendency, and each excavation step is  $30\text{ m} \times 400\text{ m}$ , and the excavation is completed in 12 steps. Currently, the commonly used contact surface method and fault zone weakening method are used to simulate fault (Chen et al. 2021). The contact surface method is to set contact surfaces between the upper and lower wall rock masses to simulate the contact between rock layers. The weakening assignment method refers to the method of simulating faults by assigning parameters to a certain area that are significantly lower than the surrounding rock mass in the simulation. Using the weakening method to simulate the fault fracture zone, the model response effect is more obvious, and its numerical value is also convenient for further research. Therefore, this article uses this method to simulate the fault zone for subsequent research. The bottom boundary and the surrounding boundary of the model constrain the boundary displacement and velocity. The top of the model is a free boundary, the initial state is self-weight equilibrium, and a trapezoidal uniform load is applied horizontally, which is 0.5 times the vertical stress. The

calculation model without fault is shown in Fig. 1a, and the calculation model with fault is shown in Fig. 1b.

### 2.2 Rock mechanics parameters

Rock is an elastic–plastic material in FLAC<sup>3D</sup>, which will be destroyed and weakened when it reaches the yield strength in the process of coal mine excavation, so the Moore-Coulomb failure criterion is adopted. The relationships between bulk modulus (*K*) and shear modulus (*G*), elastic modulus (*E*), and Poisson's ratio (*ν*) in FLAC<sup>3D</sup> are shown in Eqs. (1) and (2). The physical and mechanical property distribution of each rock stratum is shown in Table 1.

$$K = \frac{E}{3(1 - 2\nu)} \tag{1}$$

$$G = \frac{E}{2(1 + \nu)} \tag{2}$$

### 2.3 Multi-physical fields data monitoring

Figure 2 shows the layout of ground subsidence monitoring points and key strata stress monitoring points. The surface subsidence information is monitored by 50 monitoring points on the surface, and the vertical stress changes of key strata are monitored by 50 monitoring points in key strata during mining.

According to the laws of thermodynamics, energy dissipation is the essential attribute of rock deformation and failure, which reflects the continuous development of micro defects in rock, the continuous weakening of strength, and the ultimate loss process. Therefore, energy dissipation is directly related to damage and strength loss, and the amount of energy dissipation reflects the degree of initial strength attenuation (Xie 2005).

The energy relationship of rock mass element under a complex stress state is shown in Eq. (3).

$$U^d = U - U^e \tag{3}$$

**Fig. 1** Numerical calculation model and monitoring point layout **a** Numerical simulation model without faults; **b** Numerical simulation model with faults

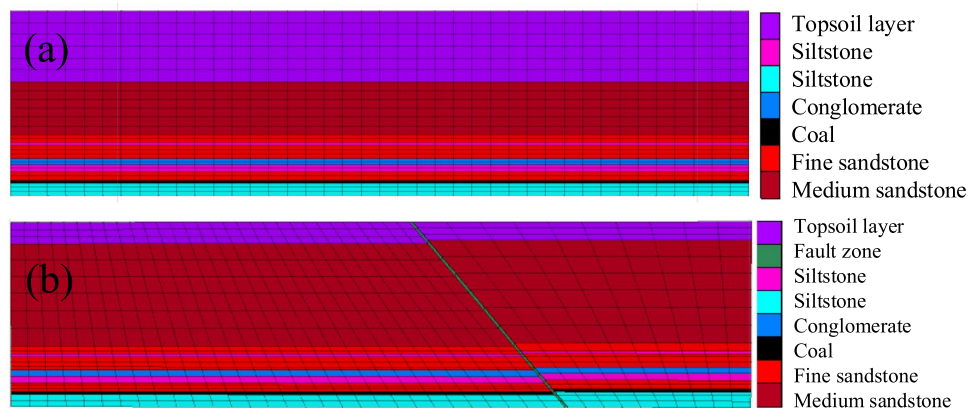
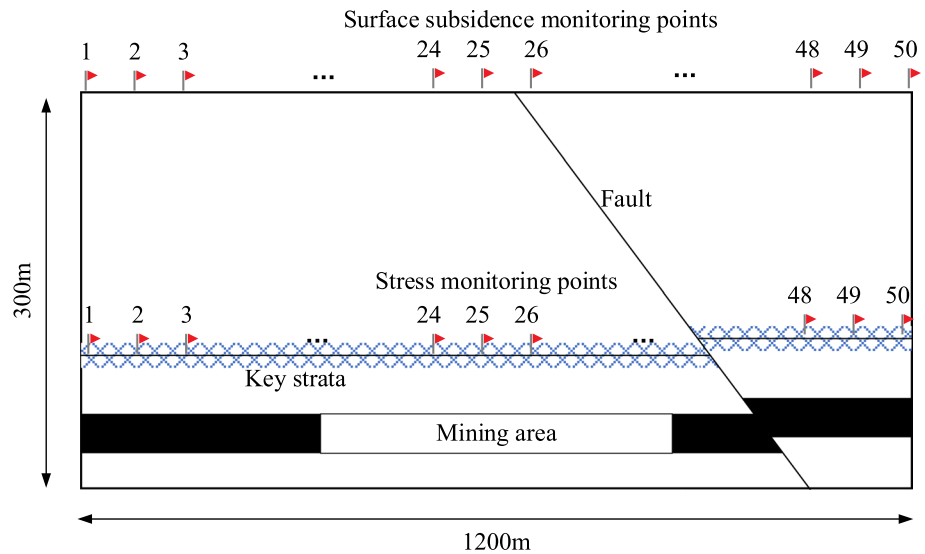


**Table 1** Mechanical parameters of each rock stratum

Lithology	Elastic modulus (GPa)	Poisson's ratio	Cohesive force (MPa)	Tensile strength (MPa)	Internal friction angle (°)
Sandstone	0.425	0.20	8.45	29.50	25
Coal	0.46	0.30	0.50	0.50	30
Fine sandstone	0.775	0.21	3.55	34.00	22
Siltstone	0.425	0.20	8.45	29.50	25
Conglomerate	1.94	0.27	16.75	32.00	29
Fine sandstone	0.775	0.21	3.55	34.00	22
Siltstone	0.425	0.20	8.45	29.50	25
Fine sandstone	0.775	0.21	3.55	34.00	22
Medium sandstone	0.69	0.26	5.15	37.20	25
Topsoil layer	0.05	0.15	0.80	20.00	35
Fault	0.05	0.2	0.25	0.25	10

**Fig. 2** Ground subsidence and critical layer stress monitoring point layout



The energy of each part of the rock mass element in the principal stress space can be expressed as Eqs. (4)–(6).

$$U = \int_0^{\epsilon_1} \sigma_1 d\epsilon_1 + \int_0^{\epsilon_2} \sigma_2 d\epsilon_2 + \int_0^{\epsilon_3} \sigma_3 d\epsilon_3 \quad (4)$$

$$U^e = \frac{1}{2E_0} \left\{ \frac{\sigma_1^2}{1-\omega_1} + \frac{\sigma_2^2}{1-\omega_2} + \frac{\sigma_3^2}{1-\omega_3} - v \left[ \left( \frac{1}{1-\omega_1} + \frac{1}{1-\omega_2} \right) \sigma_1 \sigma_2 + \left( \frac{1}{1-\omega_2} + \frac{1}{1-\omega_3} \right) \sigma_2 \sigma_3 + \left( \frac{1}{1-\omega_1} + \frac{1}{1-\omega_3} \right) \sigma_1 \sigma_3 \right] \right\} \quad (9)$$

$$U^e = \frac{1}{2} \sigma_1 \epsilon_1^e + \frac{1}{2} \sigma_2 \epsilon_2^e + \frac{1}{2} \sigma_3 \epsilon_3^e \quad (5)$$

$$\epsilon_i^e = \frac{1}{E_i} [\sigma_i - v_i (\sigma_j + \sigma_k)] \quad (6)$$

In Eqs. (3) to (6),  $U$  is the total work done by the principal stress in the principal strain direction,  $\epsilon_i^e$  is the total elastic strain in the three principal stress directions, and  $v_i$  is Poisson's ratio.

When the rock mass is undamaged in the process of failure, the energy ratio of the rock is shown in Eq. (7).

$$U^e = \frac{1}{2} \sigma_i \epsilon_i^e = \frac{1}{2} \left\{ \frac{\sigma_1^2}{E_1^2} + \frac{\sigma_2^2}{E_2^2} + \frac{\sigma_3^2}{E_3^2} - v \left[ \left( \frac{1}{E_1} + \frac{1}{E_2} \right) \sigma_1 \sigma_2 + \left( \frac{1}{E_2} + \frac{1}{E_3} \right) \sigma_2 \sigma_3 + \left( \frac{1}{E_1} + \frac{1}{E_3} \right) \sigma_1 \sigma_3 \right] \right\} \quad (7)$$

For damaged rock mass, conventional damage variables are introduced to consider the impact of damage on unloading elastic modulus  $E_i$  of rock mass, as shown in Eq. (8).

$$E_i = (1 - \omega_i) E_0 \quad (8)$$

where  $E_0$  is the initial elastic modulus of rock mass element without damage.

Assuming that Poisson's ratio  $v$  will not be affected by damage, Eq. (8) is substituted into Eq. (7) to obtain the change of elastic energy, as shown in Eq. (9).

Equation (9) is simplified for convenience of application. Let  $\bar{E} = E_0(1 - \bar{\omega})$ ,  $\bar{v} = \frac{v}{(1-\bar{\omega})}$ ,  $\omega_i = \bar{\omega}$ , ( $i = 1, 2, 3$ ).

Then the releasable elastic strain energy  $U^e$  can be rewritten as Eq. (10).

$$U^e = \frac{1}{2\bar{E}} [\sigma_1^2 + \sigma_2^2 + \sigma_3^2 - 2\bar{v}(\sigma_1 \sigma_2 + \sigma_2 \sigma_3 + \sigma_1 \sigma_3)] \quad (10)$$

According to Eq. (10), the elastic energy calculation program is compiled with fish programming language in FLAC<sup>3D</sup> to visualize the process of rock stratum energy change, and the energy change of corresponding monitoring points is sorted out.

Affected by mining, the original balance state of the coal seams near the fault is broken, and the rock stratum above the goaf collapses to form a "masonry beam" structure, as shown in the Fig. 3 (Wang et al. 2022). In Fig. 3, are the normal stress and shear stress of the fault plane, the fault dip angle, and the tectonic stress of the rock stratum.

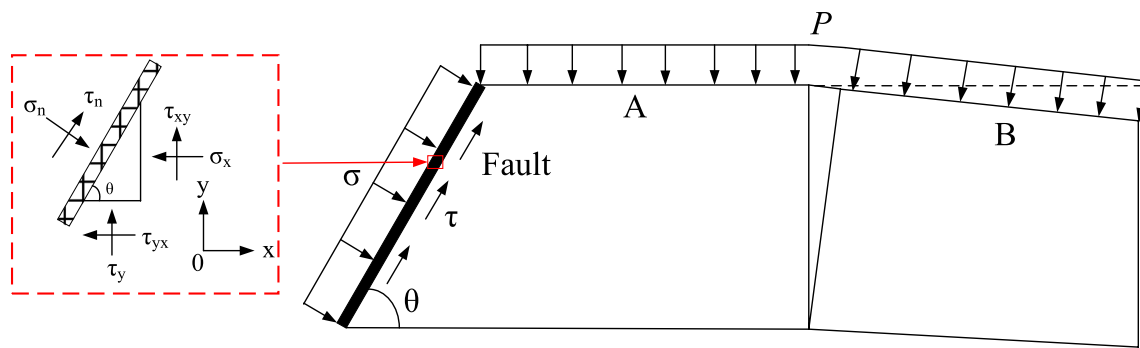


Fig. 3 Stress analysis of fault

In addition, rock block B acts on rock block A with shear force and horizontal force, and coal seam acts on rock block A with supporting stress.

Take micro units on the fault plane for analysis, as shown in Fig. 3. The micro-unit is subject to the horizontal stress  $\sigma_x$  and shear stress  $\tau_{xy}$  given by the fractured roof rock stratum, the normal stress  $\sigma_y$  and shear stress  $\tau_{yx}$  of the lower coal seam to the unit, and the mechanical analysis of the unit is conducted assuming the normal stress  $\sigma_n$  and shear stress  $\tau_n$  acting on the fault plane.  $\sigma_n$  and  $\tau_n$  are respected.

$$\sigma_n = \sigma_x \sin^2 \theta + \sigma_y \cos^2 \theta + 2\tau_{xy} \sin \theta \cos \theta \tag{11}$$

$$\tau_n = (\sigma_x - \sigma_y) \sin \theta \cos \theta + \tau_{xy} (\cos^2 \theta - \sin^2 \theta) \tag{12}$$

The stress function form of fault is shown in Eq. (13).

$$\sigma_n, \tau_n = f(\sigma_x, \sigma_y, \tau_{xy}, \theta) \tag{13}$$

It can be seen from Eq. (13) that changes caused by coal mining will lead to changes in normal stress and shear stress on the fault, and changes in the stress state of the fault will lead to activation and instability of the fault. In the following, the method of numerical simulation is used to analyze the activation trend of fault, the activation area of fault, and the change law of energy field under the influence of mining.

### 3 Results

#### 3.1 Overburden stress analysis

##### 3.1.1 Analysis of stress change of key strata under the influence of loose layer

Figure 4 shows the change of vertical stress of the key strata with an advancing distance of the working face when there is only a loose layer. Take the curve of vertical stress change

on the key strata in Fig. 4a as an example. The vertical stress curve of key strata is symmetrical about the center of the mined-out area and gradually changes from a "V" shape to a "W" shape at the early stage of mining. The vertical stress of key strata before coal mining is 6.20 MPa, with the advancing of the working face, there will be stress concentration areas on both sides of the goaf, and the stress peak value is 9.19 MPa. The stress unloading zone will be formed above the mined-out area when the coal mine in the working face is mined out, and the range of the stress unloading zone will also expand with the advancing of the working face. The stress unloading reaches the maximum when the advancing length of the working face is 180 m, and the vertical stress of the key strata is close to zero. Since then, a "stress arch" will be formed in the key strata, and the scope of the "stress arch" will gradually expand and the stress peak will gradually rise, with a maximum stress peak of 4.04 MPa.

With the thickness of the loose layer being 30, 60, 90, 120, and 150 m, respectively, the vertical stress of the key strata changes with the advancing distance of the working face as shown in Fig. 4b–f. When the thickness of the loose layer changes, the changing trend of vertical stress on the key strata is the same as that of the non-loose layer, showing the difference in stress peak value.

According to the stress monitoring results, the vertical stress of key strata after stopping mining is compared and analyzed, as shown in Fig. 5. From the figure, it can be seen that when the thickness of the loose layer changes, the stress concentration on both sides of the goaf keeps good consistency, and the stress change trend and stress concentration peak keep synchronization. The vertical stress of the key strata above the goaf presents a "W" shaped change trend, with stress concentration in the center of the goaf forming a "stress arch", and pressure relief on both sides of the goaf. The extreme stress points in the W-shaped area are divided into the minimum point  $A_1$  at 514 m, the maximum point  $B_1$  at 615 m, and the minimum point  $C_1$  at 740 m.

Further analysis of the vertical stress variation law of the "W"-shaped area formed by the key strata above the goaf,

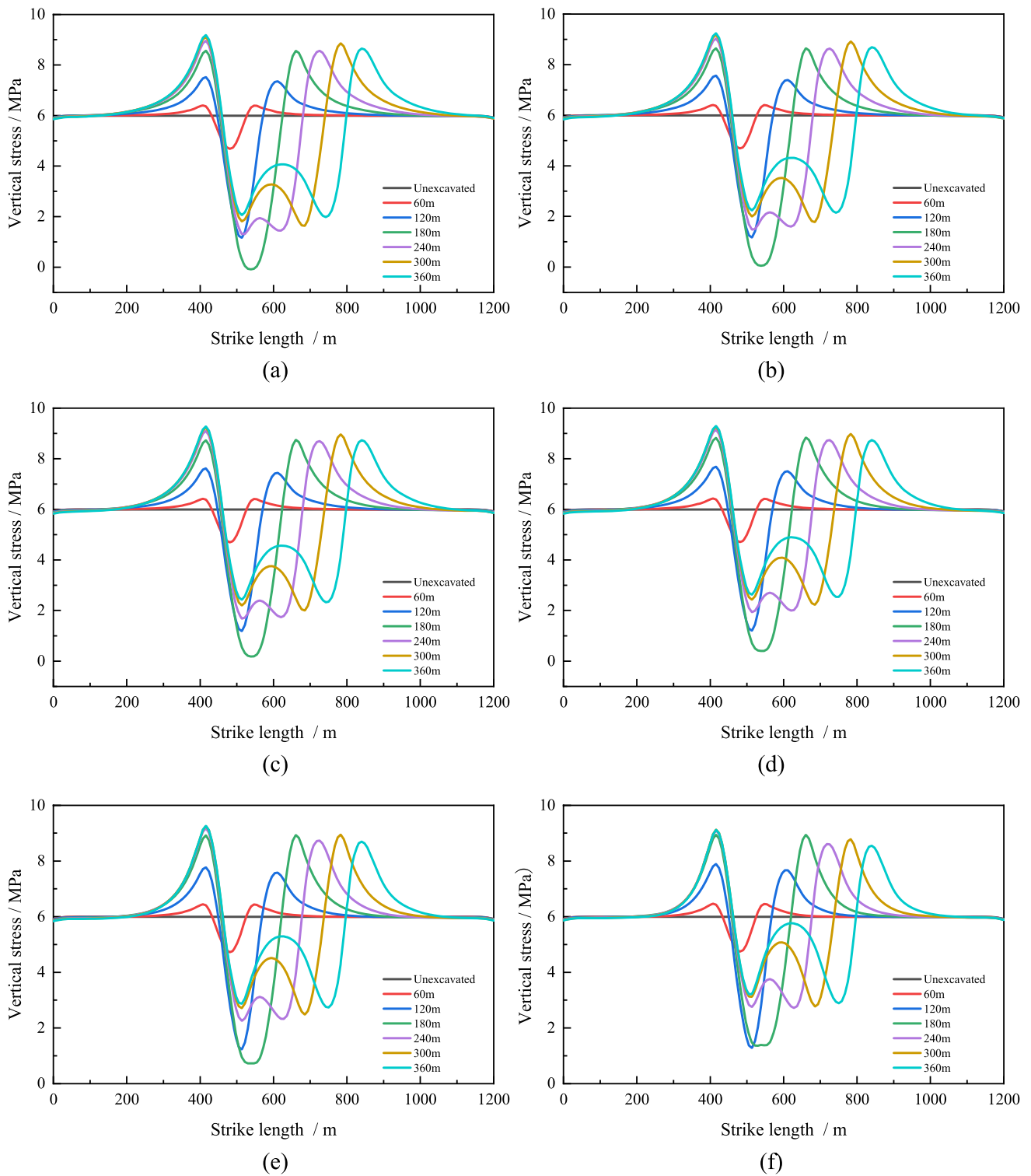


**Fig. 4** Vertical stress variation in key strata **a** No loose layer; **b** 30 m loose layer; **c** 60 m loose layer; **d** 90 m loose layer; **e** 120 m loose layer; **f** 150 m loose layer

the variation of extreme stress with the thickness of the loose layer is shown in Fig. 6. As the thickness of the loose layer increases, the stress values of  $A_1$ ,  $B_1$ , and  $C_1$  are gradually

increasing. Stress values at  $A_1$  and  $C_1$  have the same trend, and stress curves coincide. The stress value of  $A_1$ ,  $B_1$ , and  $C_1$  is 2.06 MPa, 4.05 MPa, and 2.03 MPa respectively when the

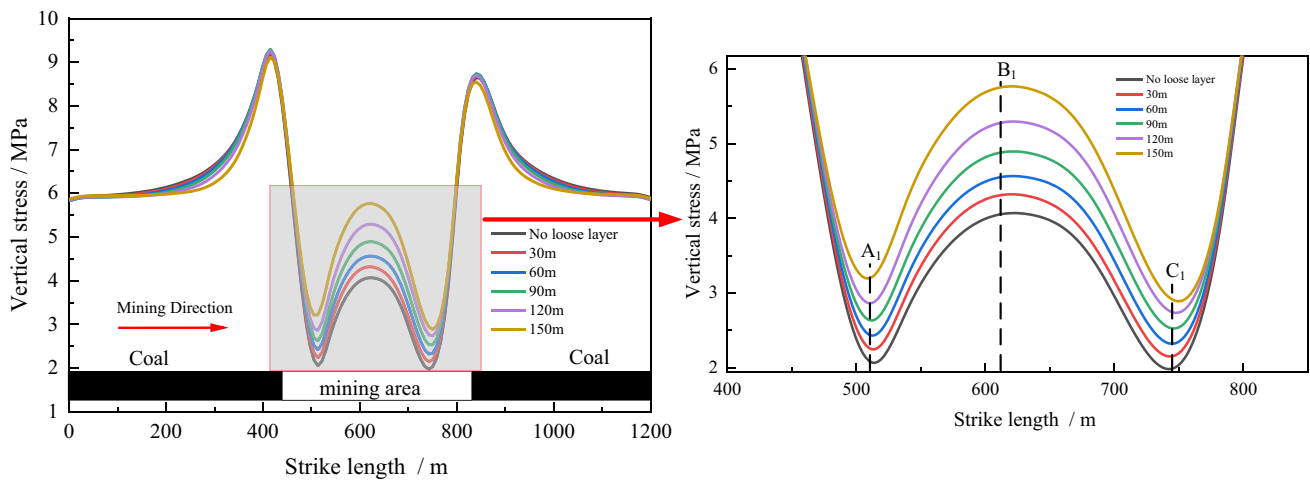


Fig. 5 Vertical stress in key strata after mining stopped

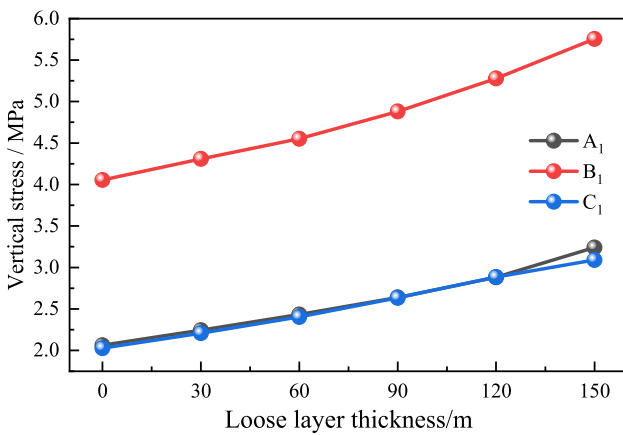


Fig. 6 Extreme stress in "W" shaped area

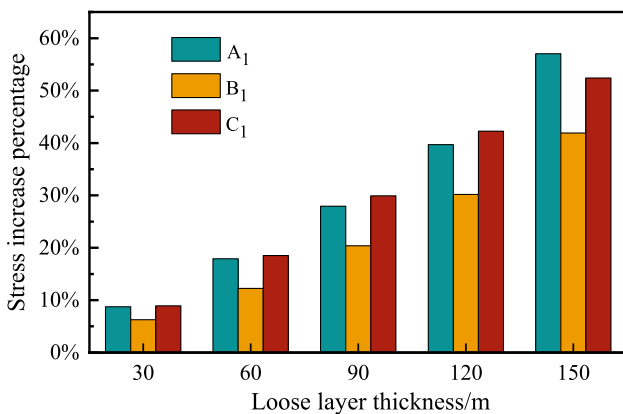
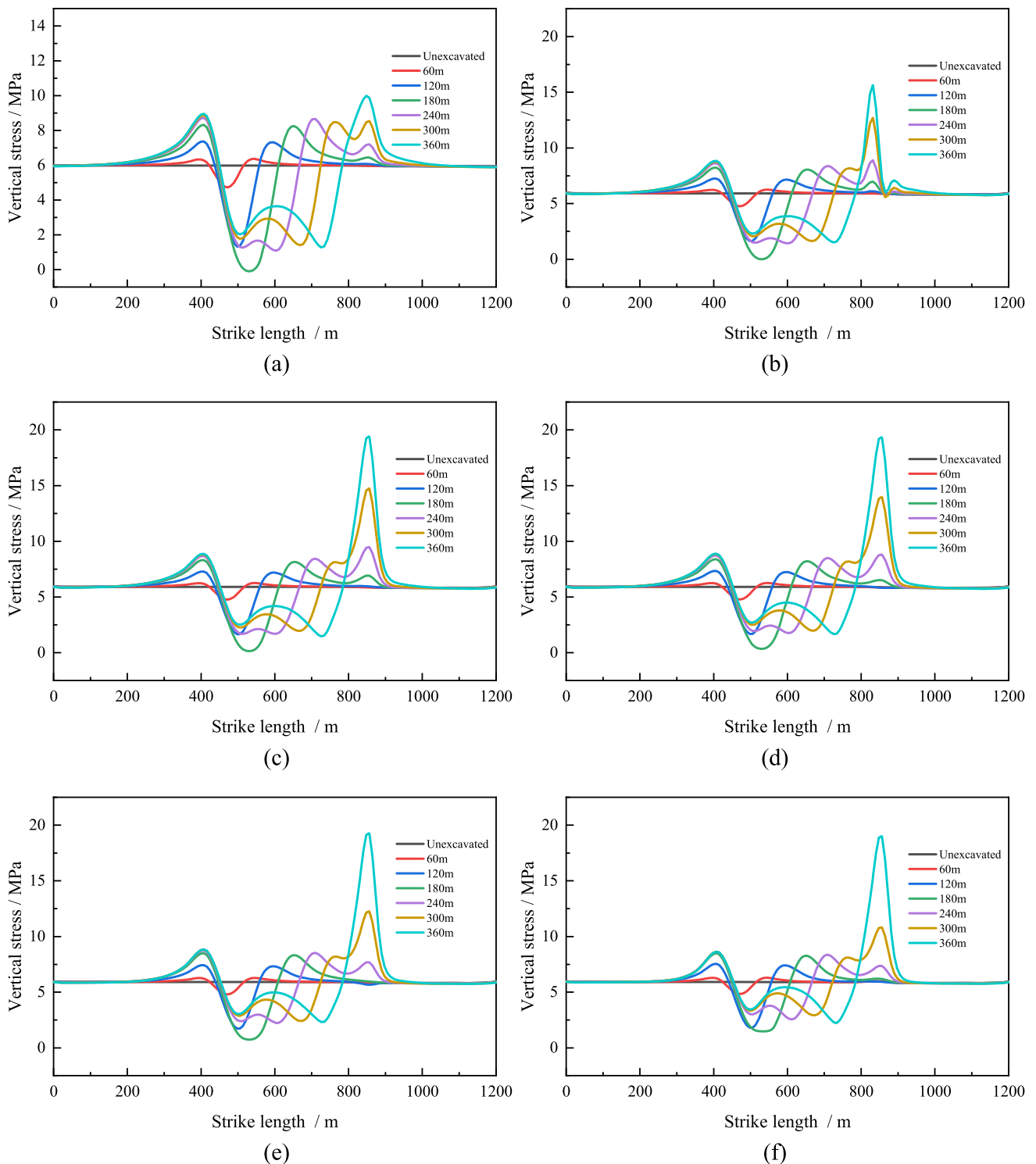


Fig. 7 Extreme stress increment in "W" shaped area

thickness of the loose layer is 0 m. The stress value of  $A_1$ ,  $B_1$ , and  $C_1$  is 3.24 MPa, 5.75 MPa, and 3.10 MPa respectively when the thickness of the loose layer is 150 m. Figure 7 shows the percentage increase of vertical stress at  $A_1$ ,  $B_1$ , and  $C_1$  when the thickness of the loose layer increases compared with that of the no-loose layer. With the thickness of the loose layer increasing from 30 to 150 m, the percentage of vertical stress increases from 8.7% to 57% at the  $A_1$  point, from 6.3% to 41.9% at the  $B_1$  point, and from 8.9% to 52.4% at  $C_1$  point. With the increase of loose layer thickness, the vertical stress of  $A_1$ ,  $B_1$ , and  $C_1$  will increase, and the vertical stress on both sides of the goaf will increase more than that in the center of the goaf.

### 3.1.2 Analysis of stress changes in key strata under the influence of coupling of loose layer and fault

When there is a fault in overburden, the change of vertical stress of key strata with the advancing distance of the working face under the influence of coupling between fault and loose layer is shown in Fig. 8. Figure 8b shows that the loose layer with a thickness of 30 m is coupled with a 55° fault. The vertical stress curve of key strata is symmetrical about the center of the goaf when the advancing distance of the working face is less than 180 m, but it will fluctuate briefly when passing through the fault. The "stress arch" will appear in the key strata above the goaf when the advancing distance of the working face is more than 180 m, and the stress concentration will appear in the area passing through the fault (870 m). The vertical



**Fig. 8** Vertical stress variation in key strata **a** No loose layer; **b** 30 m loose layer; **c** 60 m loose layer; **d** 90 m loose layer; **e** 120 m loose layer; **f** 150 m loose layer

stress of key strata gradually changes from a "V" shape to a "W" shape at the initial stage of mining, and the stress concentration occurs when it passes through the fault. The vertical stress of the key strata before mining is 5.91 MPa,

and with the advancing of the working face, stress concentration areas will appear on both sides of the goaf and near the fault, with the peak stress of 8.63 MPa on both sides of the goaf and 15.54 MPa near the fault. When the



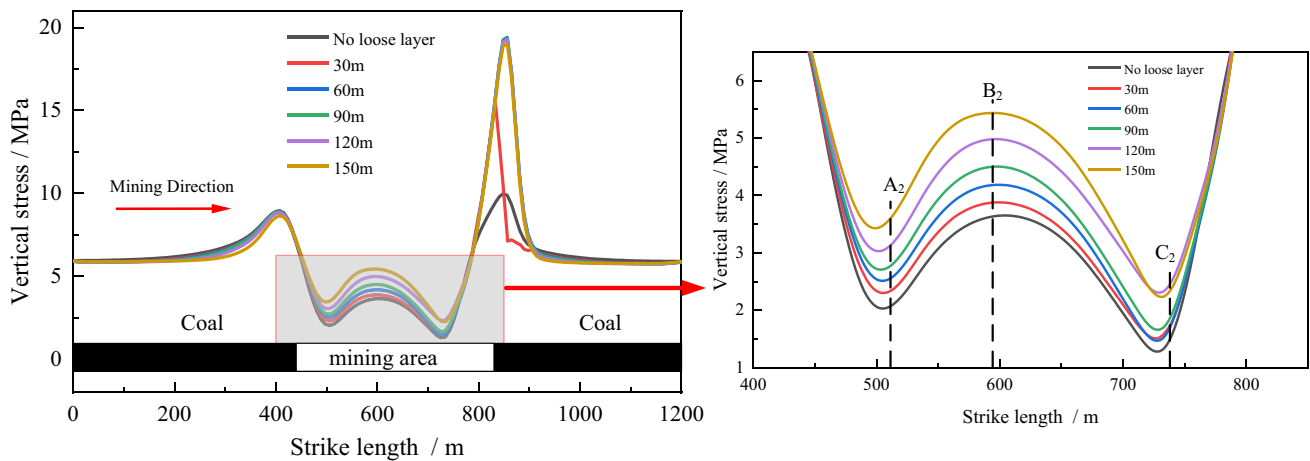


Fig. 9 Vertical stress in key strata after mining stoppage

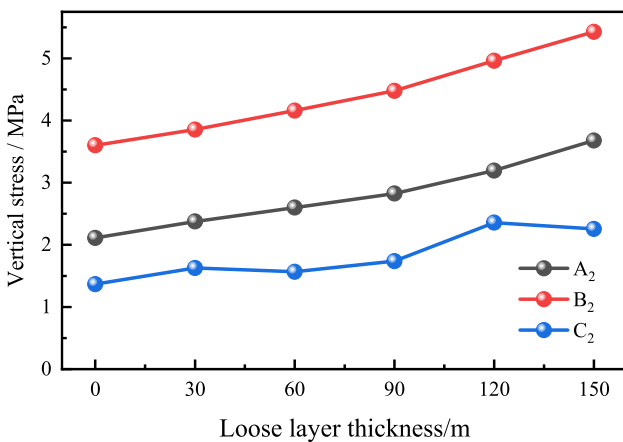


Fig. 10 Extreme stress in "W" shaped area

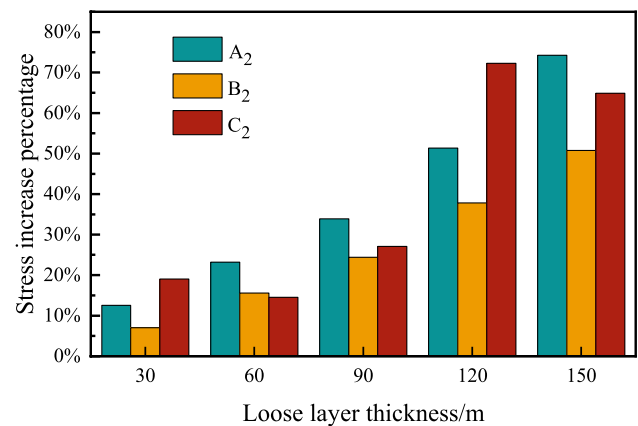
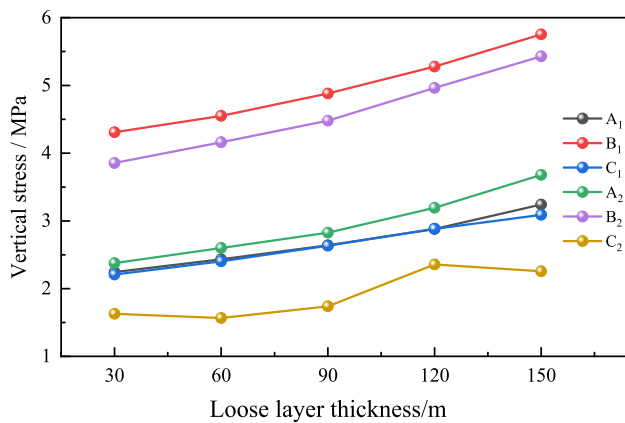


Fig. 11 Extreme stress increment in "W" shaped area

coal seam in the working face is mined, a stress unloading area will be formed above the goaf, and the scope of the stress unloading area will also expand. When the advancing length of the working face is 180 m, the stress unloading reaches the maximum, and the vertical stress of the key strata is 0.05 MPa. After that, a "stress arch" area will be formed in the key strata, and the scope and stress peak value will be gradually expanded, and the stress peak value of the "stress arch" will be 3.85 MPa.

Make a comparative analysis of the vertical stress curve when the advancing distance of the working face is 360 m, as shown in Fig. 9. It can be seen from the figure that the vertical stress of the key strata will show a "W" shape right above the goaf, resulting in pressure relief on both sides of the goaf. Stress extremum points in the "W" shaped area are divided into minimum  $A_2$  at 514 m, maximum  $B_2$  at 587 m, and minimum  $C_2$  at 740 m.

Further analysis of the vertical stress variation law of the "W" shaped area formed by the key strata above the goaf shows that the extreme point stress varies with the thickness of the loose layer as shown in Fig. 10. The stress values of points  $A_2$ ,  $B_2$ , and  $C_2$  increase with the increase of the thickness of the loose layer. The stress value of point  $B_2$  is much larger than that of points  $A_2$  and  $C_2$ , which is consistent with that of only the loose layer, and the stress change value of point  $A_2$  near the open-off cut is also higher than that of point  $C_2$  on the side of terminal line, which is different from that of the only loose layer. With the thickness of the loose layer of 30 m, the stress at  $A_2$ ,  $B_2$ , and  $C_2$  are 2.38, 3.86, and 1.63 MPa, respectively. With the thickness of the loose layer of 150 m, the stress at  $A_2$ ,  $B_2$ , and  $C_2$  are 3.68, 5.43, and 2.26 MPa, respectively. Figure 11 shows the percentage increase of vertical stress at points  $A_2$ ,  $B_2$ , and  $C_2$  when the thickness of the loose layer increases compared



**Fig. 12** Stress change at monitoring points of key strata

with that of the no-loose layer. Generally, the loose layer is loaded on the bedrock in the form of vertical static load (Wang et al. 2022). The vertical stress of  $A_2$ ,  $B_2$ , and  $C_2$  on the key layer will increase with the increase of loose layer thickness. The vertical stress of  $A_2$  and  $B_2$ , which are far away from the fault zone and less affected by the fault, shows a gradually increasing trend. Point  $C_2$  is located under the influence range of the fault, and the vertical stress will fluctuate slightly due to the influence of the fault zone. The percentage of vertical stress increases from 12.5% to 74.3% at the  $A_2$  point, from 7.1% to 50.8% at the  $B_2$  point, and from 19.0% to 64.9% at the  $C_2$  point when the thickness of the loose layer increases from 30 to 150 m. The increase of vertical stress at both sides of the goaf is greater than that at the center of the goaf.

Figure 12 shows the stress change at the extreme point of the "W" shaped area in the key strata. The figure shows that when fault exists, the vertical stress of key strata is smaller than that of no faults, and the existence of faults will hinder the propagation of stress in the overburden. The vertical stress changes in the open-off cut and goaf center are consistent, as shown in  $A_1$ ,  $A_2$ ,  $B_1$ , and  $B_2$  in Fig. 11. There are obvious differences in stress changes when the loose layer on one side of the terminal line is coupled with the fault, as shown in Fig. 12, line  $C_1$ , and line  $C_2$ . The existence of the fault on the side of the terminal line will increase the propagation obstacle of the vertical stress, so the vertical stress here will be smaller when the fault is coupled with the loose layer than when there is no fault. The fault dip angle designed in this paper is  $55^\circ$ , and the position where the fault occurs lags behind the center of the working face. In the early stage of mining, the fault will hinder the stress propagation in the whole rock stratum. When the working face reaches the fault, the hanging wall rock mass has been directly affected by the fault zone. At this time, the vertical

stress propagation of the key layer located in the fault area is blocked with greater intensity.

## 3.2 Analysis of surface subsidence

### 3.2.1 Analysis of surface subsidence under the influence of loose layer

The model with the thickness of 0 m, 30 m, 60 m, 90 m, 120 m, and 150 m of loose layer is selected to monitor the surface subsidence of the working face every 60 m. The monitoring data of surface subsidence is shown in Fig. 13. It can be seen from the figure that the surface subsidence curve of mining under conventional geological conditions is symmetrical concerning the center of the goaf. The location of the maximum subsidence point is close to the center of the goaf from the side of the open-off cut. After mining is stopped, the maximum subsidence point appears in the center of the goaf. When the thickness of the loose layer gradually increases from 0 to 150 m, the maximum surface subsidence value under the same mining length is increasing. The maximum surface subsidence values after stopping mining are 3499, 3691, 3805, 3862, 3905, and 4038 mm, respectively. When the thickness of the loose layer increases from 0 to 150 m, the maximum surface subsidence values increase by 15.4%. The subsidence values at the same location increase with the increase of the thickness of the loose layer, which shows that the promotion effect of the loose layer on surface subsidence is gradually increasing.

The thickness of the loose layer affects the base load ratio (the ratio of the thickness of the bedrock to the thickness of the loose layer) of the overlying strata on the working face (Ma et al. 2021). With the increase of the thickness of the loose layer, the thickness of the bedrock in the rock stratum decreases. Because of the special structural characteristics of the loose layer, it is loaded on the bedrock in the form of high vertical static load. Under the influence of the mining disturbance of the working face and the vertical static load of the loose layer, the damaged rock mass in the upper part of the goaf is easier to be compacted, and the separation layer between the layers tends to close gradually. The form of subsidence below the replaced rock separation layer gap is transferred to the surface, increasing the amount of subsidence on the surface.

### 3.2.2 Analysis of surface subsidence under coupling influence of loose layer and fault

Figure 14 shows the subsidence change of the surface with the advance of the working face when the loose layer with different thicknesses is coupled with the fault. It can be seen

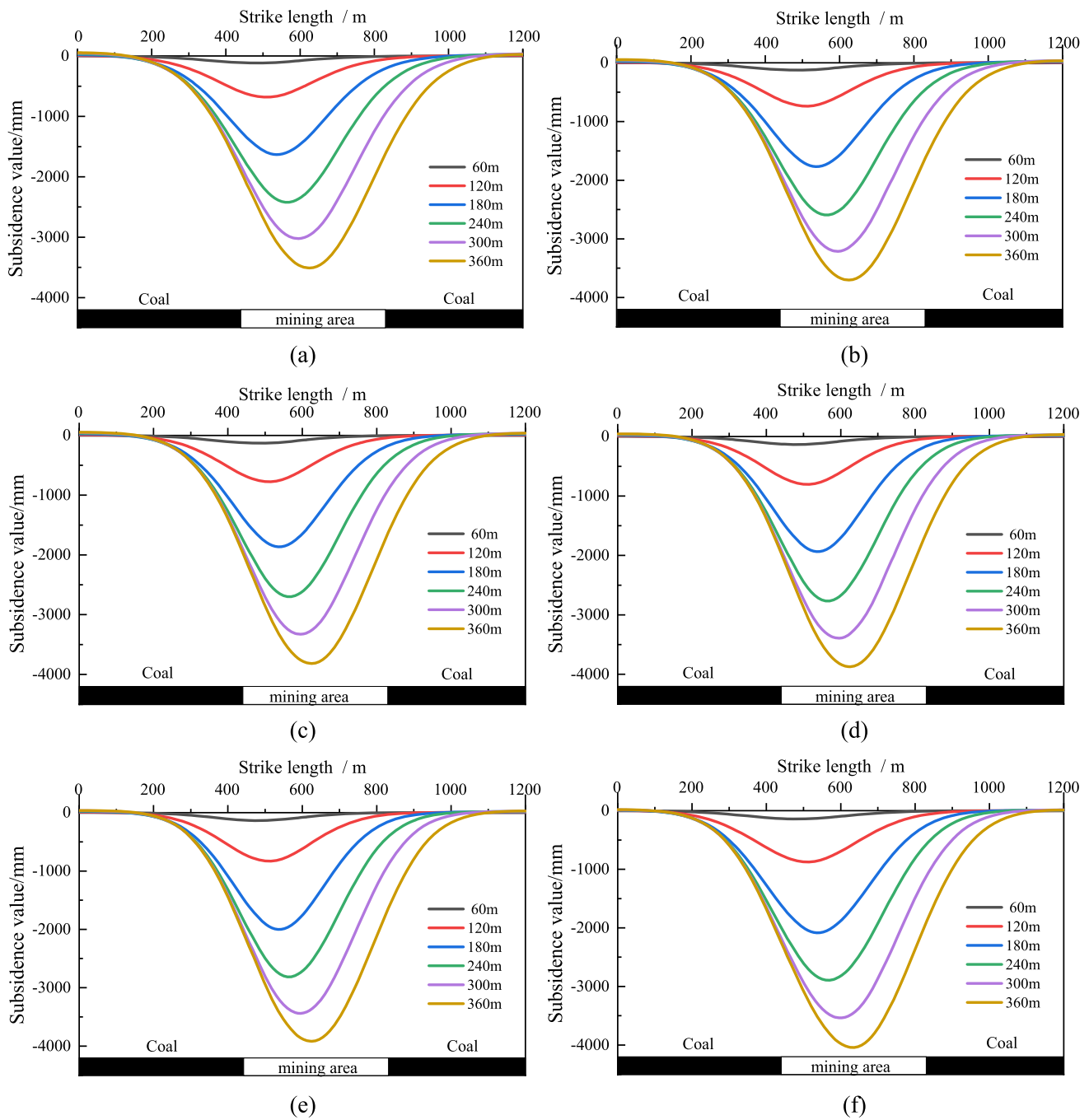


**Fig. 13** Surface subsidence with the thickness of loose layer changes **a** No loose layer; **b** 30 m loose layer; **c** 60 m loose layer; **d** 90 m loose layer; **e** 120 m loose layer; **f** 150 m loose layer

from the figure that when there is a fault in the rock stratum, the changing trend of the surface subsidence curve is no longer symmetrical about the center of the goaf, and there will be abnormal subsidence points at the fault. When the advancing length of the working face is 120 m, abnormal points begin to appear on the surface subsidence curve, and subsidence steps appear at the fault outcrop. With the advance of the working face, the maximum subsidence point

on the surface is gradually close to the center of the goaf but different from Sect. 3.2.1, the maximum subsidence point is no longer symmetrical about the center of the goaf but is offset to the side of the open-off cut. With the increase of the thickness of the loose layer, the maximum surface subsidence values after mining stoppage are 3191 , 3350, 3480, 3510, 3530, and 3580 mm, respectively. When the thickness of the loose layer increases from 0 to 150 m, the maximum

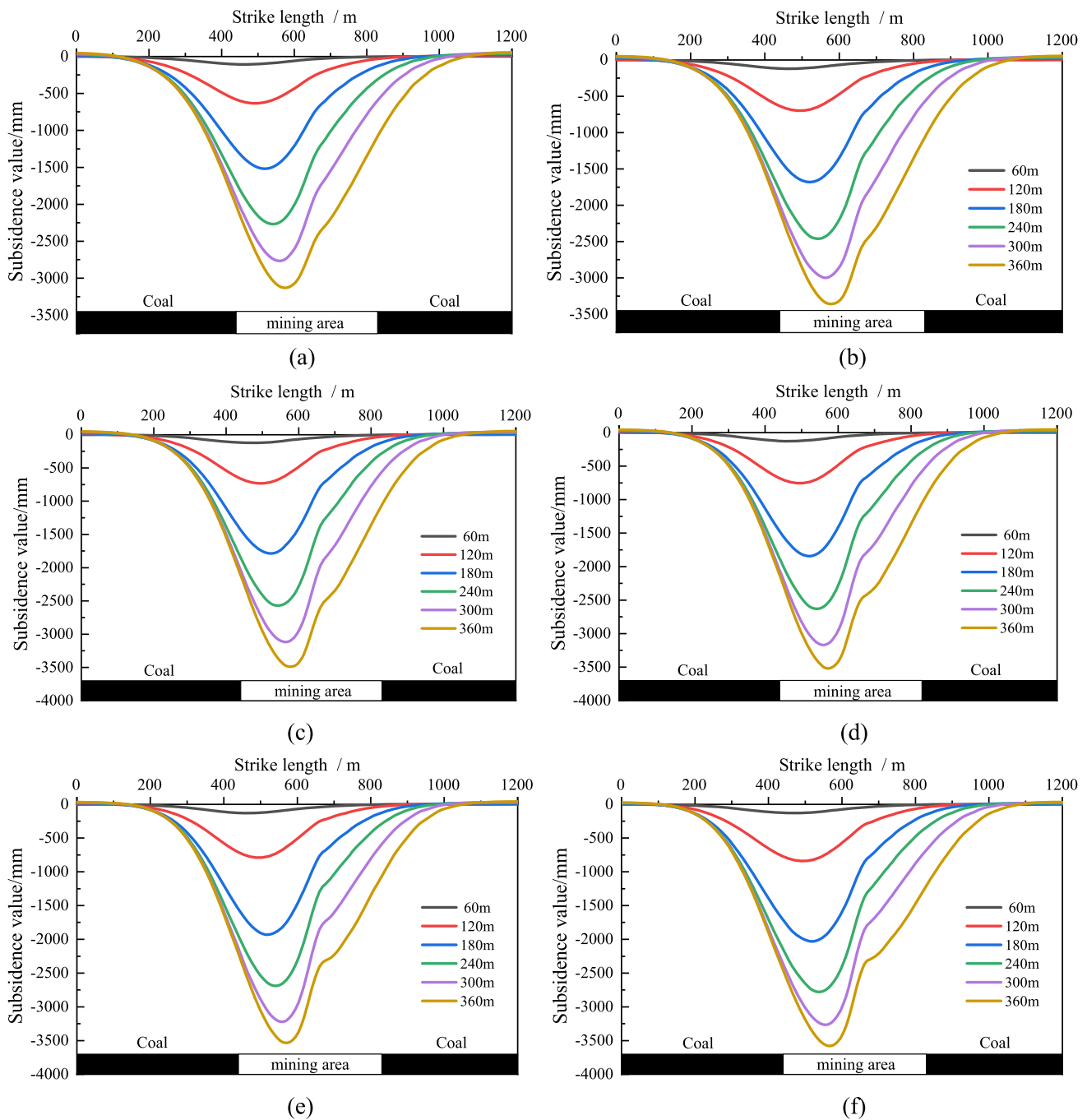


**Fig. 14** Surface subsidence with the thickness of loose layer changes **a** No loose layer; **b** 30 m loose layer; **c** 60 m loose layer; **d** 90 m loose layer; **e** 120 m loose layer; **f** 150 m loose layer

surface subsidence increases by 12.2%, which is weakened under the action of faults.

The mechanism of discontinuous surface deformation is that a weak surface releases mining vertical stress and shear stress through its medium, making the rock mass at the side of the weak surface far from goaf less affected by mining (Dudek et al. 2020). As a weak surface in the rock stratum, the fault zone acts as a barrier to the movement of

the rock stratum, destroying the continuity of the internal rock stratum subsidence, so there will be abnormal points in the surface subsidence. The increase in the thickness of the loose layer will make the bedrock bear a higher vertical static load, and the existence of faults can weaken the rock movement caused by the increase in the thickness of the loose layer. The linkage evolution of loose layer and fault is always in the process of dynamic change, and during

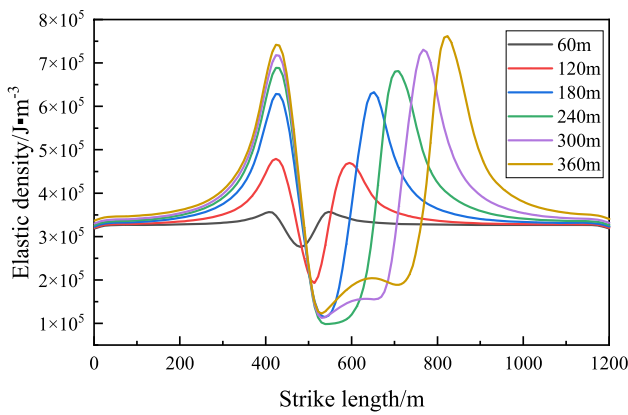


**Fig. 15** Elastic energy of 30 m thick loose bed varies with mining length

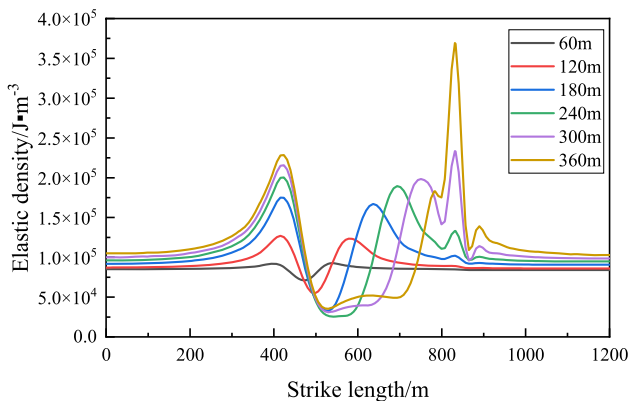


**Fig. 16** Variation of elastic energy of coupling 30 m loose layer and fault with mining length

this period, it is also affected by many factors, such as rock stratum combination, tectonic movement, and mining layout. This process is extremely complex. When the loose layer and fault are coupled, the linkage evolution process between them can be described as follows: (1) When there is no loose layer and the thin loose layer above the working face, the fault plays a leading role in surface subsidence. At this time, the fault will block the spread of overburden stress, resulting in abnormal surface subsidence on the fault side. (2) When there is a thick loose layer above the working face, the fault and loose layer play a similar leading role in surface subsidence. Thick loose layer will lead to greater surface subsidence, while the fault will hinder surface subsidence. (3) When there is an extra-thick loose layer in the working face, the loose and unstable structure of the very thick loose layer will aggravate the surface subsidence. At this time, the blocking effect of the fault on the surface subsidence is not enough to offset the promoting effect of the extra-thick loose layer.

### 3.3 Energy change analysis

#### 3.3.1 Energy change law of key strata

Figures 15 and 16 respectively show the evolution process of elastic energy of key strata with mining length when there is only loose layer and loose layer is coupled with fault. It can be seen from Figs. 15 and 16 that the elastic strain energy accumulation effect will occur in the strata on both sides of the goaf. The energy dissipation effect appears in the area above the goaf, the elastic strain energy is lower than the initial energy value, and the energy dissipation degree in the center of the goaf is the largest. When the mining length reaches 300 m, the energy in the center of the goaf rises again. When there is only loose layer, the changing trend of the elastic properties of the key strata under the same mining length is symmetrical about the center of the goaf. With the increase of mining length, the energy accumulation occurs near the open-off cut, and the energy accumulation position at the end of the goaf is gradually far away from the open-off cut.

Under the coupling effect of loose layer and fault, when the mining length is less than 240 m, the changing trend of the elastic property of key strata is consistent with the working condition where only loose layer exists. When the mining length reaches 240 m, the elastic strain energy of the monitoring point near the fault will drop suddenly, then increase rapidly, after reaching the maximum value, it will drop suddenly, and after a short period of fluctuation, it will gradually become stable. According to the analysis of the vertical stress of the key strata in Sect. 3.1, the changing trend of the elastic properties of the key strata is synchronized with the change trend of the vertical stress on the key strata.

From the analysis of the data of energy change, it can be seen that the initial elastic strain energy at the key strata is  $3.3 \times 10^5$  J when there is only loose layer, the maximum value of energy accumulation at the open-off cut side is  $7.37 \times 10^5$  J, and the maximum value of energy accumulation at the terminal line side is  $7.46 \times 10^5$  J. When the loose layer is coupled with the fault, the initial elastic energy at the key strata is  $8.6 \times 10^4$  J, the maximum value of energy accumulation at the open-off cut side is  $2.38 \times 10^4$  J, and the maximum value of energy accumulation at the terminal line side is  $3.68 \times 10^4$  J. The initial elastic performance of the key strata, the maximum accumulated elastic performance of the open-off cut, and the maximum accumulated elastic energy of the terminal line under the condition of loose layer only are 3.8 times, 3.1 times, and 2.0 times of those under the coupling effect of loose layer and fault respectively. The existence of a fault when the fault is coupled with a loose layer will reduce the elastic energy on the key strata.

### 3.3.2 Fault zone elastic energy evolution characteristics

According to the above analysis, faults will cause the elastic energy on the key strata to decrease, while the energy is always conserved during the mining process. The resistance of the fault to the stress propagation leads to a large amount of energy accumulating in the fault and the overlying strata. A large number of studies show that the rock burst caused by the fault has gone through this process (Wang et al. 2021), and the energy change of the fault and the nearby coal and rock gradually changes from a stable accumulation state to an unstable release state. Due to the influence of many factors such as high-stress levels in coal and rock, the special geological structure of fault, and mining conditions, the energy change of coal and rock during mining has obvious space–time characteristics.

This article has studied the elastic energy evolution law on the 55° fault zone when the thickness of the loose layer changes. Due to the limited space of the article, to quantify the elastic energy evolution law, this section selects the

incremental analysis of the elastic energy change along the fault zone with the mining length when the thickness of the loose layer is 60 m. When the loose layer is coupled with the fault zone, the characteristics of the elastic energy change on the fault zone are shown in Fig. 17. According to the analysis of Fig. 17a, the elastic performance of the fault zone is mainly accumulated in the shallowly buried fault at the initial stage of mining, and the elastic energy increment of the fault zone presents a "Bowl" shape. At this time, the maximum elastic energy accumulation increment of the shallow buried fault zone is  $1.6 \times 10^4$  J. With the increase of mining length, the accumulation of elastic energy is gradually transferred to the deep fault, and the accumulation range of elastic energy is gradually increased. As shown in Fig. 16e, the maximum elastic energy accumulation is  $3.0 \times 10^6$  J, and the elastic energy accumulation has increased 187 times.

In the process of coal mining, the overlying strata will move, deform and destroy. As the working face advances, the deformation of overlying strata will gradually develop upward, which will lead to the dynamic response of the stope

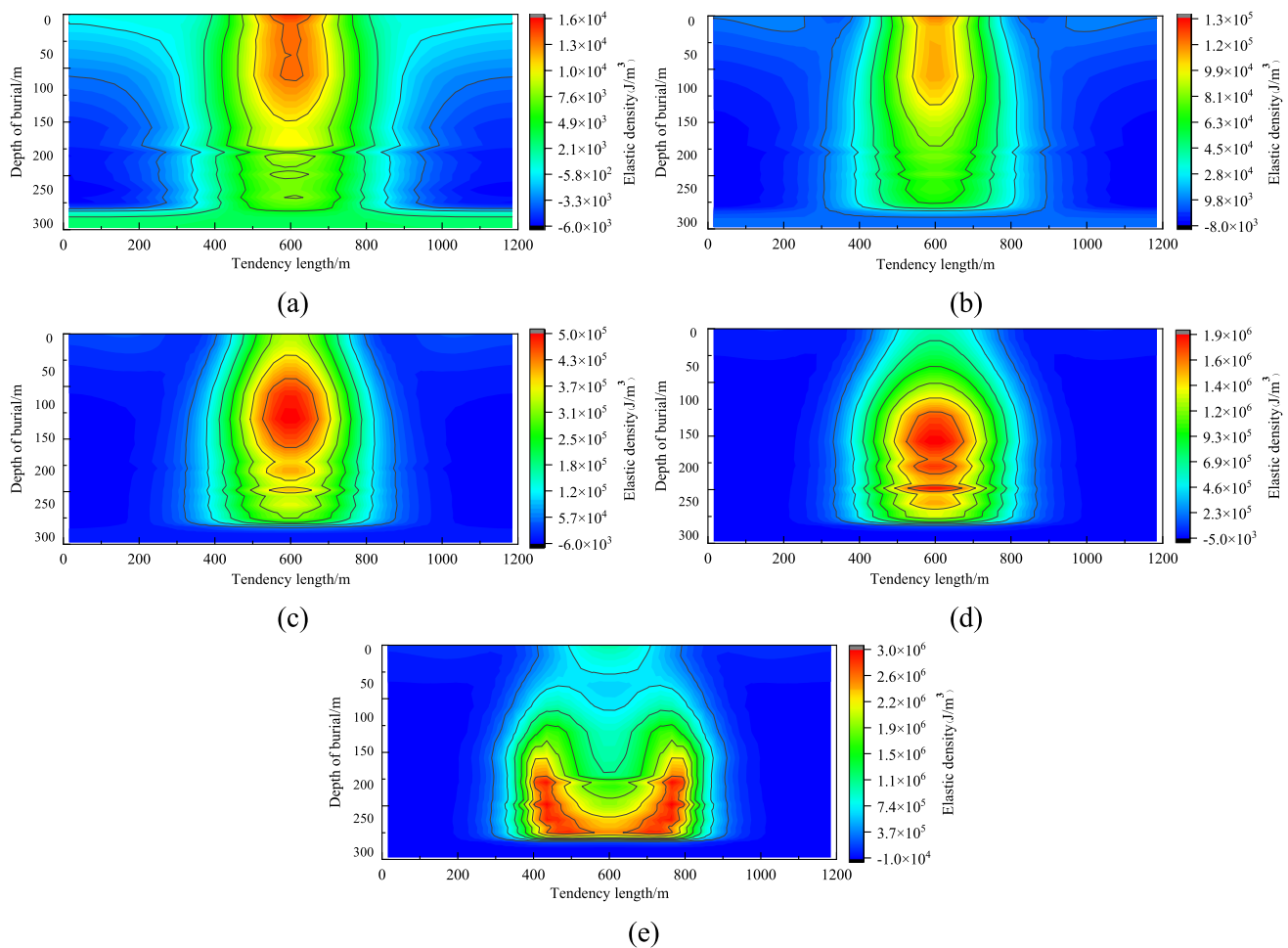


**Fig. 17** Fault zone elastic energy distribution. Advance length of working face: **a** 120 m; **b** 180 m; **c** 240 m; **d** 300 m; **e** 360 m

and the surface (Guo et al. 2020). At the initial stage of mining, the working face is far away from the fault zone, and the mining activity of the working face cannot affect the stability of the fault. However, due to the particularity of the loose layer structure, the shallow coal seam is vulnerable to mining. With the advance of the working face, the shallowly buried fault is first affected and becomes unstable, and the stable structure of the activated unstable fault zone is broken, which is no longer having the function of accumulating energy. When the working face is pushed close to the fault, the deeply buried fault zone can still maintain a complete structure relying on the bonding of surrounding rock masses. At this time, a large amount of energy will be accumulated in the middle fault to create conditions for subsequent activation and sliding. During the mining process, the fault will accumulate energy at the shallowly buried fault first. After the shallowly buried fault is destroyed, it will no longer have the function of accumulating energy. The location of elastic energy accumulation will gradually transfer to the middle fault. After the middle fault accumulates enough energy and is destroyed, the elastic energy accumulation will gradually shift to the fault zone with greater burial depth, and finally, the complete structure of the entire fault zone will be destroyed.

### 3.4 Fault zone slip analysis

According to relevant research, when the stress on the fault zone changes and the stress of a node in the fault zone exceeds its ultimate strength, the node will be damaged (Sainoki and Mitri 2014). The activated unstable area of the fault zone is extracted with fish language. The activated unstable area of the fault zone at different distances from working faces with different loose layer thicknesses to the fault zone during mining is shown in Fig. 18. When the working face is 165 m away from the fault zone, the initial stress balance of

the fault zone is broken, and the fault zone starts to activate and become unstable. At this time, the fault zone is in the initial stage of activation. When the working face is 120 m away from the fault zone, the area where the fault zone is activated and becomes unstable suddenly increases. At this time, the fault zone is in the stage of intensified activation. When the working face is 90 m away from the fault zone, the activated area of the fault zone is still increasing gradually, but it can be seen from the activated unstable area of the fault zone that the growth rate of the activated unstable area of the fault zone is decreasing, and the fault zone is in the stable stage of activation. The fault activation becomes unstable and goes through the initial activation stage, the intensified activation stage, and the stable activation stage.

Furthermore, the activated unstable area of the fault zone in the mining process is analyzed. In the initial stage of activation, the fault zone without loose layer, 30 m, 60 m, and 90 m loose layer took the lead in active slip. Under the working conditions of 120 m and 150 m loose layer, the active slip of the fault zone has a certain hysteresis, and the fault zone starts to slip when the working face is 150 m away from the fault zone. In the intensified activation stage, the activated instability area of the fault zone is bounded by the working condition of no loose layer. Under the working conditions of 30 m and 60 m loose layers, the activated instability area of the fault zone is greater than that of 90 m, 120 m, and 150 m loose layers. The activated instability area of the fault zone is 4 times that of the initial activation stage. In the stable activation stage, the increase rate of the activated unstable area of the fault zone slows down. The activated unstable area of the fault zone under the 60 m, 90 m, and 120 m loose layers is equivalent, and the activated unstable area of the fault zone under the 30 m and 150 m loose layers is equivalent. The activated unstable area of the fault zone is the smallest when there is no loose layer.

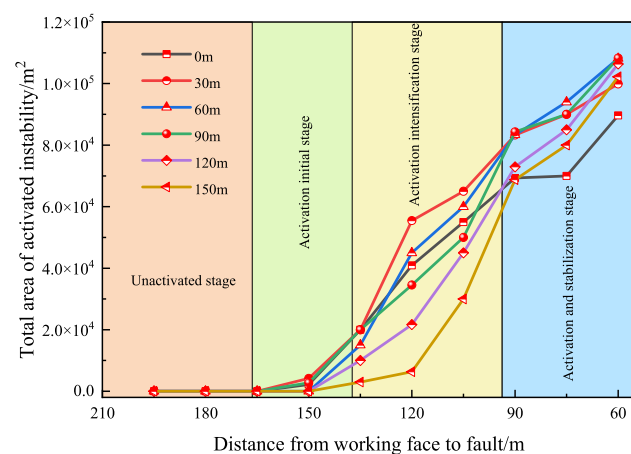


Fig. 18 Fault activation area

## 4 Conclusions

Given the important role of loose layer and fault in stress evolution and surface subsidence, this paper studies the evolution characteristics of multi-physical fields of overburden under the coupling of loose layer and fault. The following conclusions can be drawn through monitoring the vertical stress of key strata, surface subsidence, fault zone energy, and fault zone activated slip area.

- (1) Only under the action of loose layer, does the vertical stress change trend of key strata gradually change from a "V" shape to a "W" shape at the beginning of mining. Stress concentration areas appear on both sides of the goaf. When the coal seams in the working face are mined out, a stress unloading area will be formed above

the goaf. When the loose layer is coupled with the fault, the vertical stress of the key strata gradually changes from the "V" shape to the "W" shape at the beginning of mining, and the stress concentration occurs when passing through the fault.

- (2) The interaction between the loose layer and the fault affects the surface subsidence. When there is no loose layer above the rock stratum and when there is a thin loose layer, the fault plays a dominant role in surface subsidence. When there is a thick loose layer above the rock stratum, the leading role of the fault and loose layer on surface subsidence is comparable. When there is an extra-thick loose layer on the working face, the loose and unstable structure of the huge thick loose layer will intensify the surface subsidence, and the obstructing effect of the fault on the surface subsidence is not enough to offset the promoting effect of the huge thick loose layer, and then an extra-thick loose layer plays a leading role in the surface subsidence.
- (3) The elastic energy on the key strata is mainly concentrated on both sides of the goaf, and the elastic energy in the center of the goaf is dissipated. When the loose layer is coupled with the fault, the elastic energy accumulation on the key strata is less than that in the loose layer only. At the initial stage of mining, the elastic energy accumulation of the fault zone first appears in the shallow fault zone, and the elastic energy increment of the fault zone presents a "Bowl" shape. With the increase of mining length, the elastic energy accumulation gradually transfers to the deep fault zone, and the elastic energy accumulation range is also gradually increasing.
- (4) The active instability of fault is induced by mining. When the working face is 165 m away from the fault zone, the fault zone starts to be activated and unstable, and the fault zone is at the initial stage of activation. When the working face is 120 m away from the fault zone, the fault zone is in the stage of activation and intensification. When the working face is 90 m away from the fault zone, the fault zone is in the active and stable stage. Fault activation destabilization goes through the activation initial stage—activation intensification stage—activation smooth stage. The activation slip occurs first in fault zones without a loose layer, thin loose layer, and thick loose layer working conditions, and there is a certain lag in the activation slip of fault zones under the action of the extra-thick thick loose layer.

**Acknowledgements** We thank the editors and reviewers for providing very helpful comments on the manuscript.

**Authors contributions** All authors contributed to the study's conception and design. Material preparation, data collection, and analysis were performed by Jin Luo and Qingbiao Guo. The first draft of the manuscript was written by Jin Luo and all authors commented on previous versions of the manuscript. All authors read and approved the final manuscript.

**Funding** This work is supported by the Natural Science Foundation of China (52274164, 52174102), the Anhui Province Key Research and Development Plan Project (2022m07020007).

**Availability of data and materials** The datasets used or analysed during the current study are available from the corresponding author on reasonable request.

## Declarations

**Competing interests** The authors declared that they have no conflict of interest.

**Open Access** This article is licensed under a Creative Commons Attribution 4.0 International License, which permits use, sharing, adaptation, distribution and reproduction in any medium or format, as long as you give appropriate credit to the original author(s) and the source, provide a link to the Creative Commons licence, and indicate if changes were made. The images or other third party material in this article are included in the article's Creative Commons licence, unless indicated otherwise in a credit line to the material. If material is not included in the article's Creative Commons licence and your intended use is not permitted by statutory regulation or exceeds the permitted use, you will need to obtain permission directly from the copyright holder. To view a copy of this licence, visit <http://creativecommons.org/licenses/by/4.0/>.

## References

- Brunori CA, Bignami C, Albano M, Zucca Samsonov S, Gropelli G, Stramondo S (2015) Land subsidence, ground fissures, and buried faults: InSAR monitoring of Ciudad Guzmán (Jalisco, Mexico). *Remote Sens* 7(7):8610–8630. <https://doi.org/10.3390/rs70708610>
- Cai W, Dou L, Si G, Hu Y (2021) Fault-induced coal burst mechanism under mining-induced static and dynamic stresses. *Engineering* 7(5):687–700. <https://doi.org/10.1016/j.eng.2020.03.017>
- Cao Z, Gu Q, Huang Z, Fu J (2022) Risk assessment of fault water inrush during deep mining. *Int J Mining Sci Technol* 32(2):423–434. <https://doi.org/10.1016/j.ijmst.2022.01.005>
- Chen SJ, Xiao M, Wang XW (2021) Numerical analysis of seismic damage characteristics of an underground cavern intersected by a steeply dipped fault. *Rock Soil Mech* 42(9):2600–2610
- Cui G, Zhang C, Ye J, Zhou H, Li L, Zhang L (2022) Influences of dynamic normal disturbance and initial shear stress on fault activation characteristics. *Geomech Geophys Geo-Energy Geo-Resour* 8(5):1–15. <https://doi.org/10.1007/s40948-022-00463-6>
- Dudek M, Tajduś K, Misa R, Sroka A (2020) Predicting of land surface uplift caused by the flooding of underground coal mines—A case study. *Int J Rock Mech Min Sci* 132:104377. <https://doi.org/10.1016/j.ijrmms.2020.104377>
- Fernández-Torres EA, Cabral-Cano E, Novelo-Casanova DA, Havazli Solano-Rojas D, E, Salazar-Tlaczani L, (2022) Risk assessment of land subsidence and associated faulting in Mexico City using InSAR. *Natl Hazards* 112(1):37–55. <https://doi.org/10.1007/s11069-021-05171-0>



- Garcia FE, Bray JD (2022) Discrete element analysis of earthquake surface fault rupture through layered media. *Soil Dyn Earthq Eng* 152:107021. <https://doi.org/10.1016/j.soildyn.2021.107021>
- Guo WB, Bai EH, Zhao GB (2020) Current status and progress on overburden and surface damage and prevention technology of high-intensity mining. *J China Coal Soc* 45(2):509–523
- Jiang L, Kong P, Shu J, Fan K (2019) Numerical analysis of support designs based on a case study of a longwall entry. *Rock Mech Rock Eng* 52(9):3373–3384. <https://doi.org/10.1007/s00603-018-1728-2>
- Jiang L, Wu Q, Wu Q, Wang P, Xue Y, Kong P, Gong B (2019) Fracture failure analysis of hard and thick key layer and its dynamic response characteristics. *Eng Failure Anal* 98:118–130. <https://doi.org/10.1016/j.engfailanal.2019.01.008>
- Jiang Q, Yan F, Wu J, Fan Q, Li S, Xu D (2019) Grading opening and shearing deformation of deep outward-dip shear belts inside high slope: a case study. *Eng Geol* 250:113–129. <https://doi.org/10.1016/j.enggeo.2019.01.018>
- Lai XP, Zhang XD, Shan PF, Cui F, Liu BW (2021) Study on development law of water-conducting fractures in overlying strata of three soft coal seam mining under thick loose layers. *Chinese J Rock Mech Eng* 40(9):1739–1750
- Lu CP, Liu Y, Wang HY, Liu PF (2016) Microseismic signals of double-layer hard and thick igneous strata separation and fracturing. *Int J Coal Geol* 160:28–41. <https://doi.org/10.1016/j.coal.2016.04.011>
- Ma J, Yin D, Jiang N, Wang S, Yao D (2021) Application of a superposition model to evaluate surface asymmetric settlement in a mining area with thick bedrock and thin loose layer. *J Clean Prod* 314:128075. <https://doi.org/10.1016/j.jclepro.2021.128075>
- Rahmatmand B, Tahmasebi A, Lomas H, Honeyands T, Koshy P, Hockings K, Jayasekara A (2023) A technical review on coke rate and quality in low-carbon blast furnace ironmaking. *Fuel* 336:127077. <https://doi.org/10.1016/j.fuel.2022.127077>
- Rehbock-Sander M, Jesel T (2018) Fault induced rock bursts and micro-tremors—experiences from the Gotthard base tunnel. *Tunnell Undergr Space Technol* 81:358–366. <https://doi.org/10.1016/j.tust.2018.07.003>
- Sainoki A, Mitri HS (2014) Dynamic behaviour of mining-induced fault slip. *Int J Rock Mech Min Sci* 66:19–29. <https://doi.org/10.1016/j.ijrmms.2013.12.003>
- Ścigala R, Szafulera K (2020) Linear discontinuous deformations created on the surface as an effect of underground mining and local geological conditions—case study. *Bull Eng Geol Environ* 79(4):2059–2068. <https://doi.org/10.1007/s10064-019-01681-1>
- Shen B, Duan Y, Luo X, van de Werken M, Dlamini B, Chen L, Canbulat I (2020) Monitoring and modelling stress state near major geological structures in an underground coal mine for coal burst assessment. *Int J Rock Mech Min Sci* 129:104294. <https://doi.org/10.1016/j.ijrmms.2020.104294>
- Shoaib K, Zafar ZA, Raja ZA, Burley SD (2022) Ratana field, potwar fold belt, northern pakistan: high intensity fracture zones related to major thrust faults as revealed by seismic fracture prediction. *J Pet Geol* 45(3):253–282. <https://doi.org/10.1111/jpg.12819>
- Souque C, Knipe RJ, Davies RK, Jones P, Welch MJ, Lorenz J (2019) Fracture corridors and fault reactivation: example from the Chalk, Isle of Thanet, Kent, England. *J Struct Geol* 122:11–26. <https://doi.org/10.1016/j.jsg.2018.12.004>
- Wang F, Chen SJ, Ren MZ, Xu J (2019) Effect of arch structure in unconsolidated layers on failure of the overlying strata. *J China Univ Min Technol* 48(5):975–983
- Wang XB, Guo CS, Deng CQ (2020) Numerical modeling of fault barrier effects on three kinds of stresses: a case of footwall mining on the normal fault. *Progress Geophys* 35(4):1605–1611
- Wang H, Shi R, Deng D, Cui F, Jiang Y (2021) A calculation methodology of fault relative displacement used to study the mechanical characteristic of fault slip. *J Geophys Eng* 18(6):920–942. <https://doi.org/10.1093/jge/gxab063>
- Wang TX, Cao MH, Jiang HD (2022) Study on law of fault activation failure and energy release under influence of mining. *Coal Sci Technol* 50(07):75–83
- Wu Q, Wu Q, Xue Y, Kong P, Gong B (2018) Analysis of overlying strata movement and disaster-causing effects of coal mining face under the action of hard thick magmatic rock. *Processes* 6(9):150. <https://doi.org/10.3390/pr6090150>
- Xie HP, Ju Y (2005) Li LY (2005) Criteria for strength and structural failure of rocks based on energy dissipation and energy release principles. *China J Rock Mech Eng* 17:3003–3010
- Zhou D, Wu K, Li L, Diao X, Kong X (2016) A new methodology for studying the spreading process of mining subsidence in rock mass and alluvial soil: an example from the Huainan coal mine, China. *Bull Eng Geol Environ* 75(3):1067–1087. <https://doi.org/10.1007/s10064-016-0877-3>

**Publisher's Note** Springer Nature remains neutral with regard to jurisdictional claims in published maps and institutional affiliations.